中国科学院近代物理研究所
Institute of Modern Physics, CAS

ECRIS 2020

Influences of Magnetic Field Parameters on ECRIS Plasma Characteristics

J. Li[1]

L. X. Li[1,2]**, B. S. Bhaskar**[3,4]**, V. Toivanen**[3]**, O. Tarvainen**[3,5]**, D. Hitz**[1]**, L. B. Li**[1]**, W. Lu**[1]**, H. Koivisto**[3]**, T. Thuillier**[4]**, J. W. Guo**[1]**, X. Z. Zhang**[1,2]**, H. Y. Zhao**[1,2]**, L. T. Sun**[1,2] **and H. W. Zhao**[1,2]

[1]Institute of Modern Physics (IMP), Chinese Academy of Sciences, Lanzhou 730000, China
[2]School of Nuclear Science and Technology, University of Chinese Academy of Sciences, Beijing 100049, China
[3]University of Jyväskylä, Department of Physics (JYFL), 40500 Jyväskylä, Finland
[4]Laboratoire de Physique Subatomique et de Cosmologie, 53 avenue des Martyrs, 38026 Grenoble Cedex, France
[5]STFC ISIS Pulsed Spallation Neutron and Muon Facility, Rutherford Appleton Laboratory, Harwell, OX110QX, UK

The 24th International Workshop on ECR Ion Source
East Lansing, USA, September 28th, 2020

Outline

I. Quick overview

II. Experimental setup

III. Investigation and results

IV. Discussion and conclusion

Quick overview

- **Correlation of magnetic field parameters to bremsstrahlung spectral temperature T_s is not yet clear**

minimum magnetic field B_{min} and gradient at resonance zone ∇B_{ecr} are key parameters on T_s

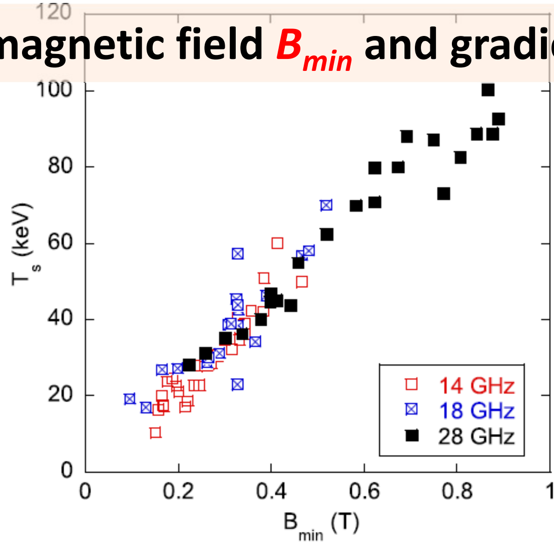

Benitez J et al 2017 IEEE Trans. Plasma Sci. 45 1746–54

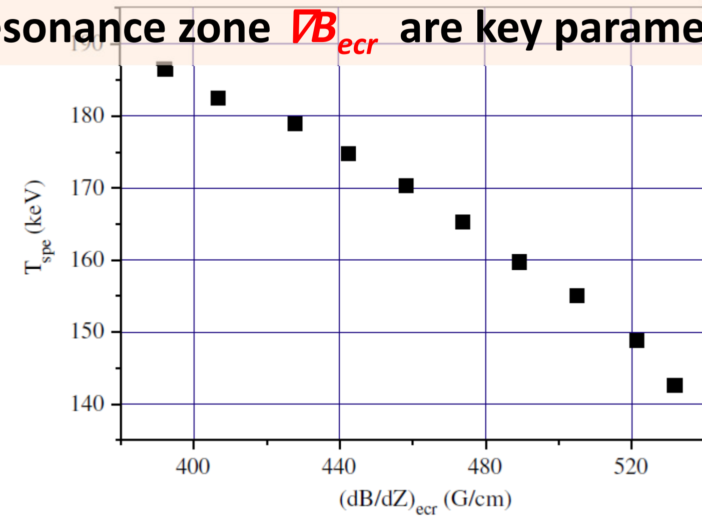

Zhao H Y et al 2009 Plasma Sources Sci. Technol. 18 025021

- **Possible correlation between bremsstrahlung spectra and the appearance of electron cyclotron instabilities are still unknown**

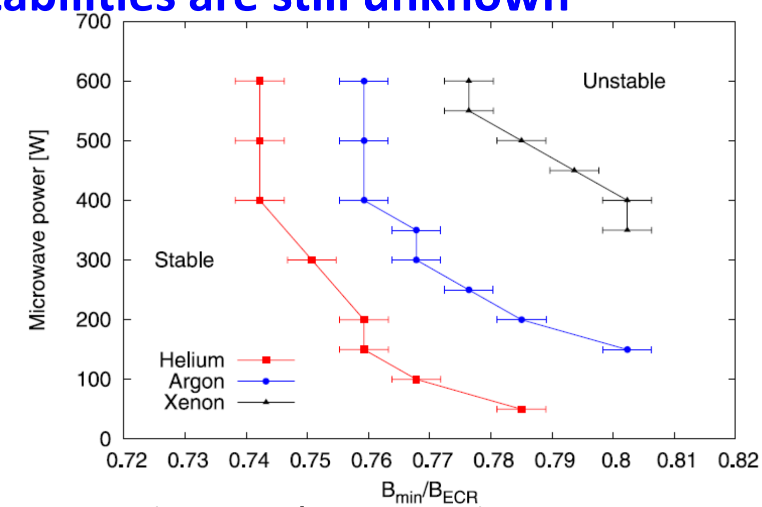

Tarvainen O et al 2016 Rev. Sci. Instrum. 87 02A703

SECRAL-II ion source

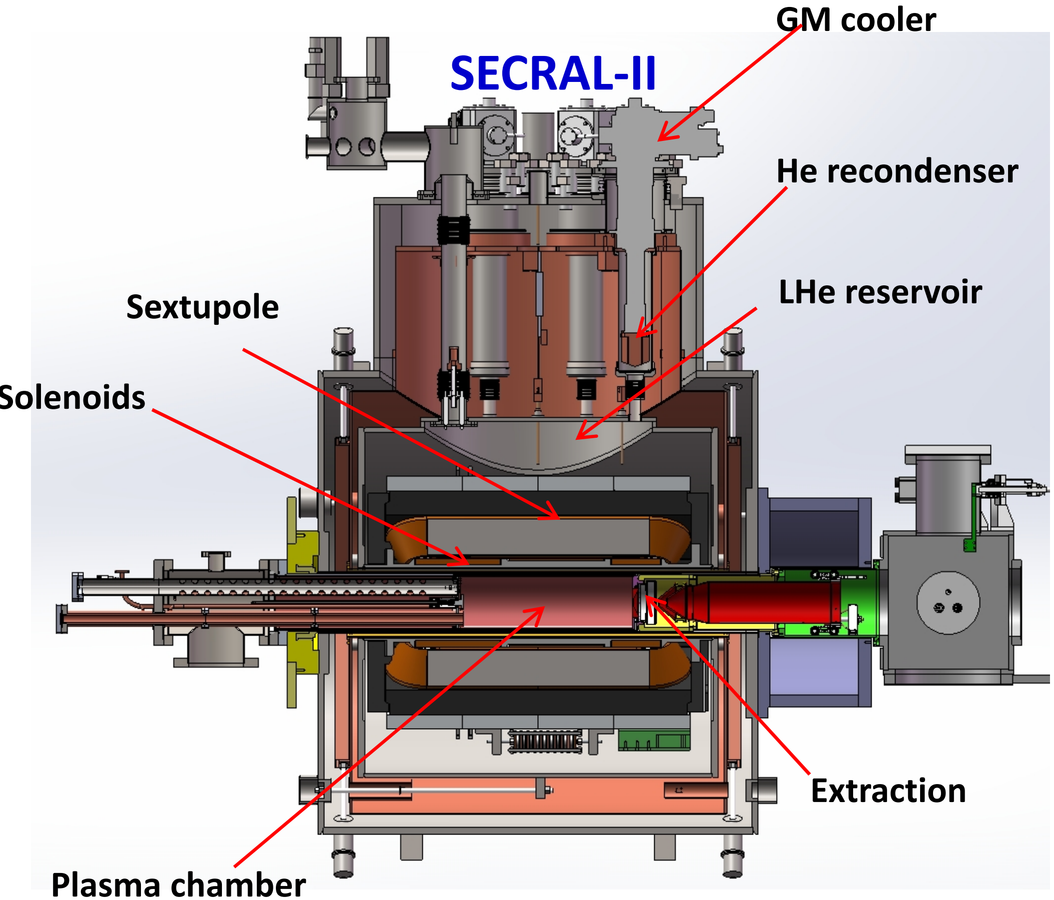

Key parameters

ω_{rf} (GHz)	18-28
Axial Field Peaks (T)	3.7 (Inj.), 2.2 (Ext.)
Mirror Length (mm)	420
No. of Axial SNs	3
B_r at Chamber Inner Wall (T)	2.0
Magnet Cooling	LHe bathing
Chamber ID (mm)	125.0
Dynamic cooling power (W)	~6

Bremsstrahlung detection system

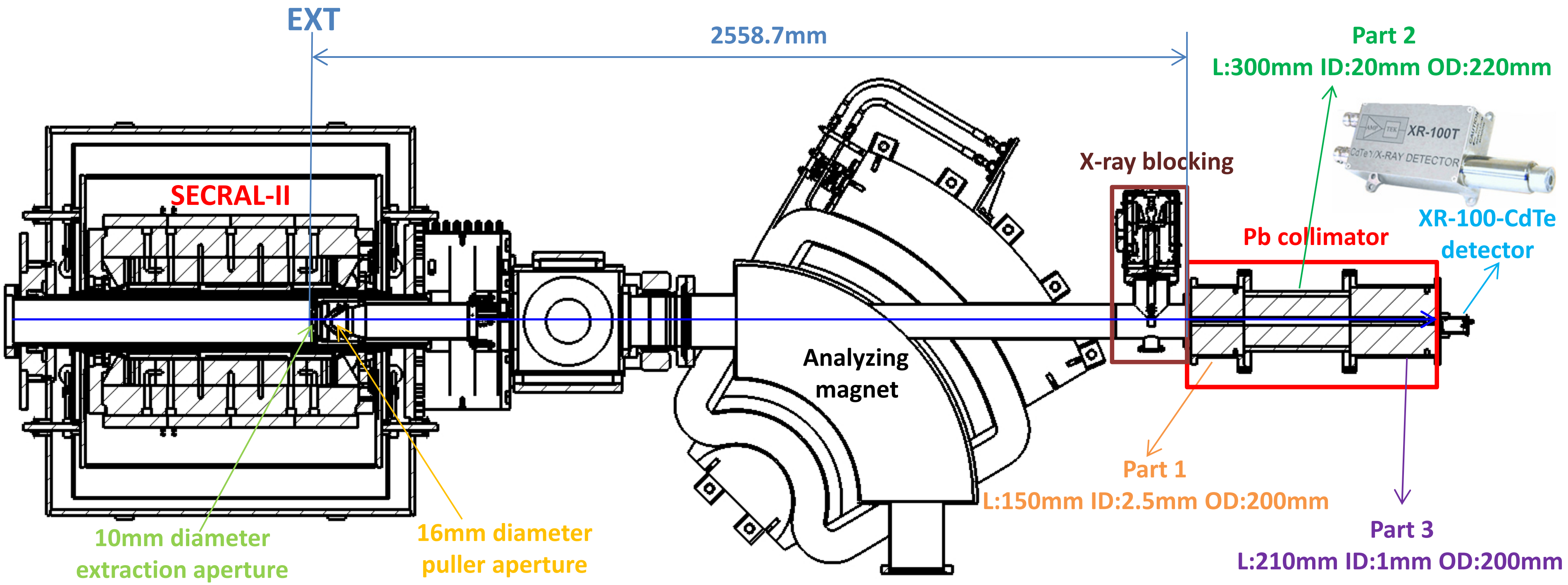

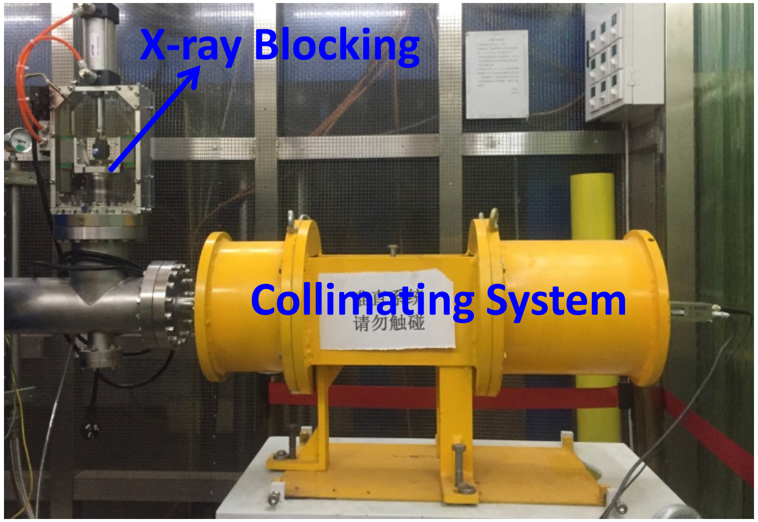

- ☐ Designed using **MCNP** code to avoid
  - I. Thick target bremsstrahlung
  - II. Secondary radiation

Spectral temperature T_s determination

I. Calibration applied

II. Spectra corrected for detector efficiency

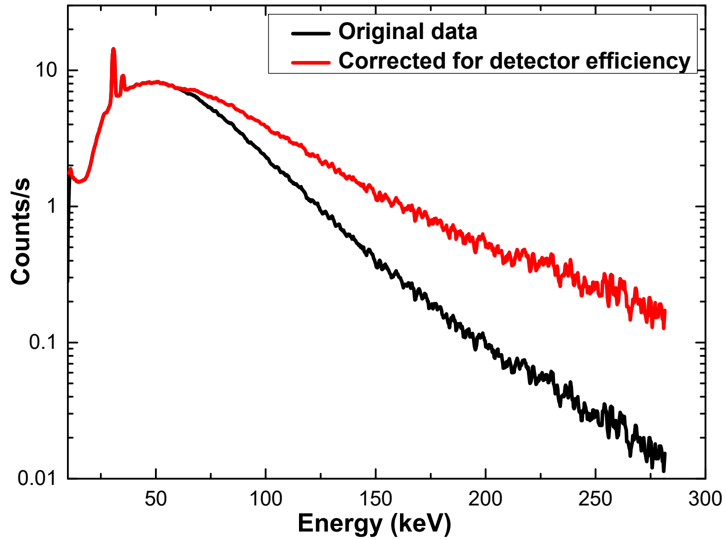

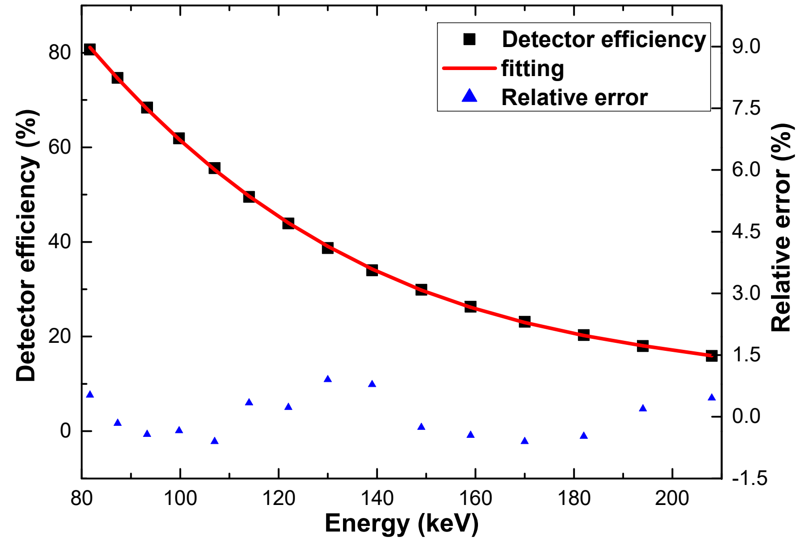

III. Linear fit applied

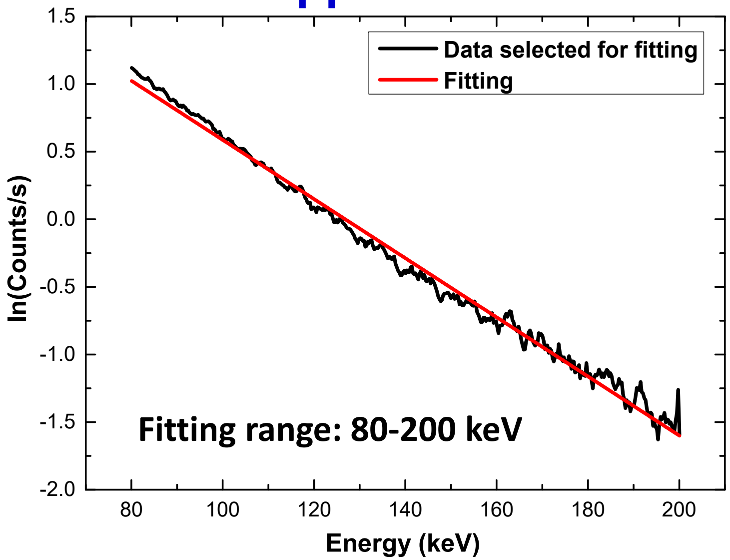

$$Spectral\ Power\ \ j(\hbar\omega) \propto \ \exp(-\hbar\omega / T_s)$$

In semi-log plot

T_s=-1/slope

Microwave signal measurement system

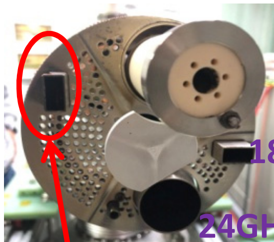

18GHz injection

24GHz injection

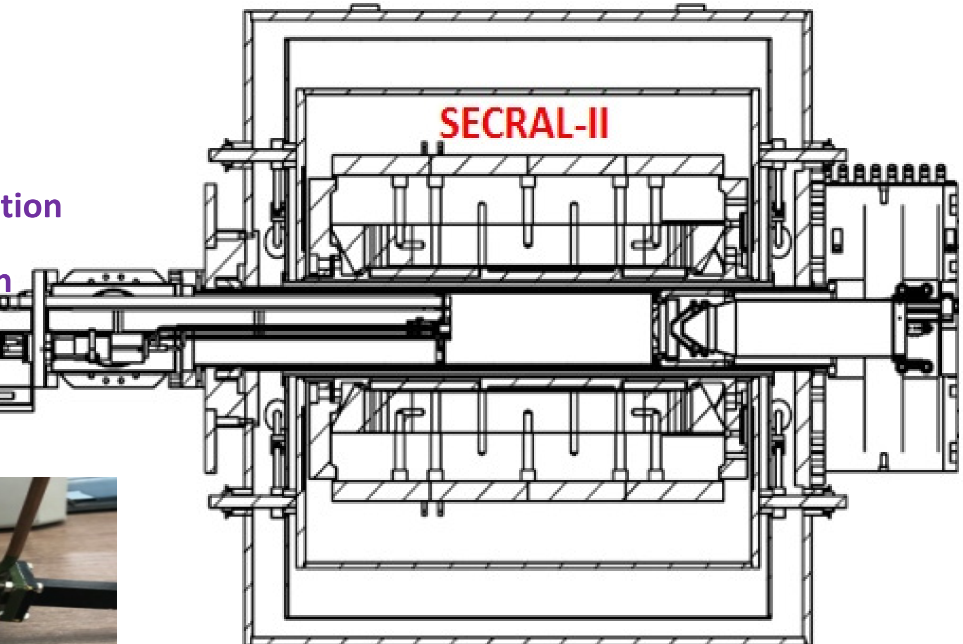

WR62

HV break

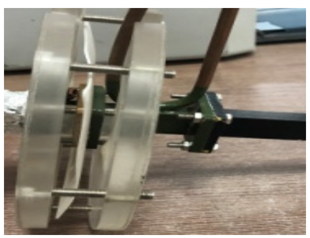

0.01-26.5 GHz
Schottky Diode Detector

WG to coax → Attenuator → Detector → Oscilloscope

Electron cyclotron instabilities

- Driven by **hot electrons** interacting resonantly with electromagnetic plasma waves
- A characteristic feature (independent on the mode) is **emission of microwaves**
- Energy of microwave emission, E_μ, is described by growth and damping rates, Γ and Δ

$$\frac{dE_\mu}{dt} \approx (\Gamma - \Delta) E_\mu$$

Γ is proportional to the anisotropy of the EVDF

$$\Gamma \propto \frac{n_{e,hot}}{n_{e,cold}}$$

Exponential growth of instability amplitude when Γ > Δ

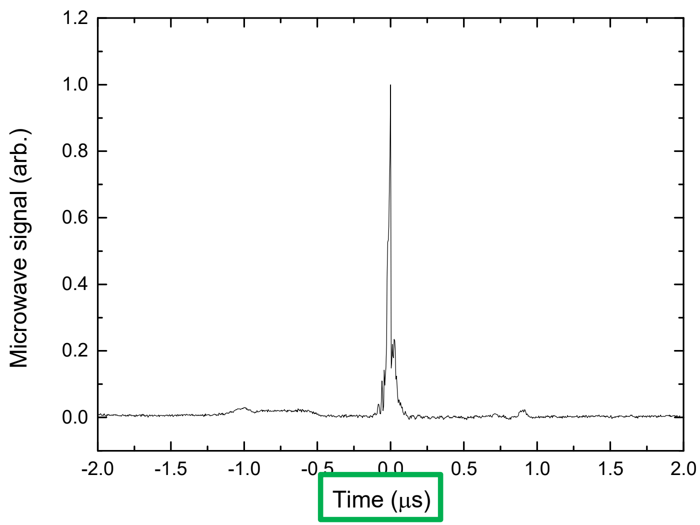

Example of microwave signal associated with electron cyclotron instability on SECRAL-II

Source parameters

Beam	Xe
Frequency (GHz)	18、24
Power (w)	1500
Extraction Voltage (kV)	20
Biased Disk Voltage (-V)	40-50
Injection Pressure (mbar)	1~2x10^{-7}

Experimental results- part 1
Constant B_{inj} , B_{ext} and B_r while varying B_{min}

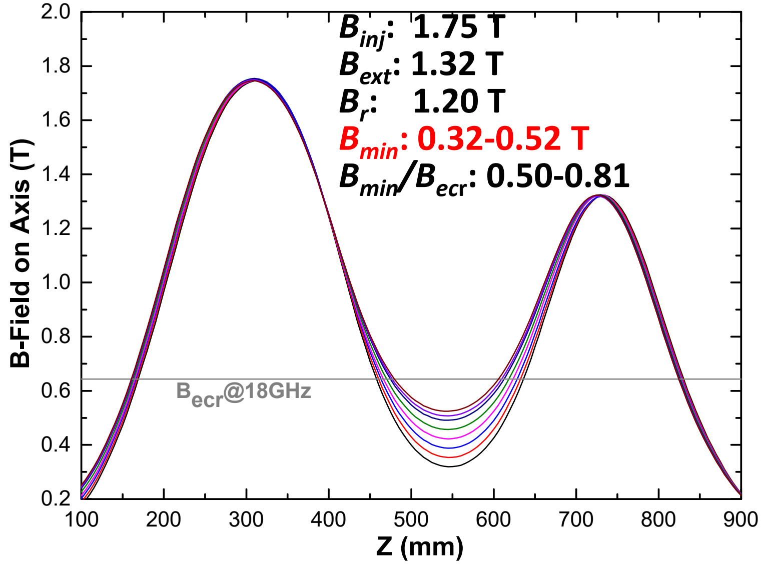

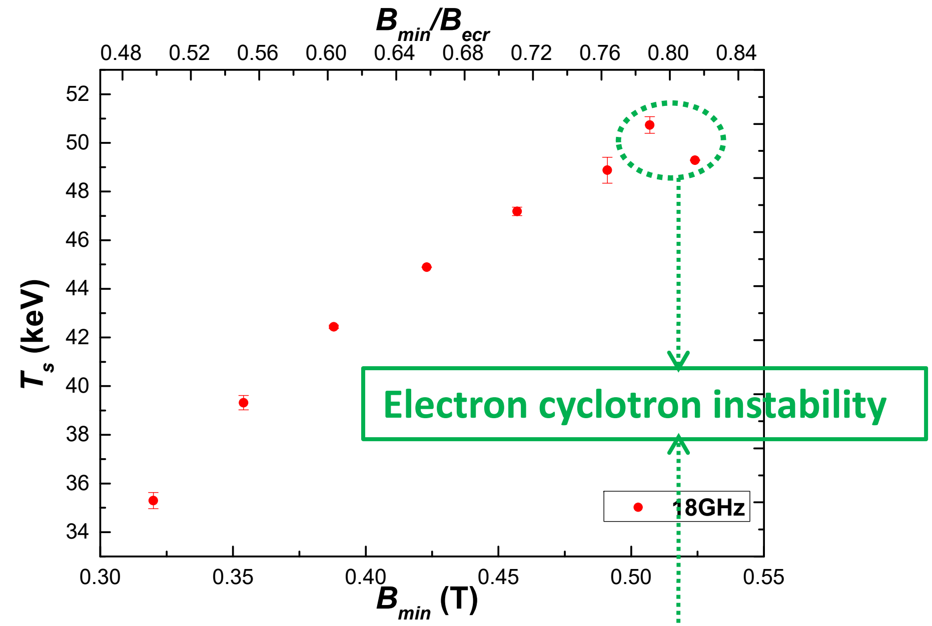

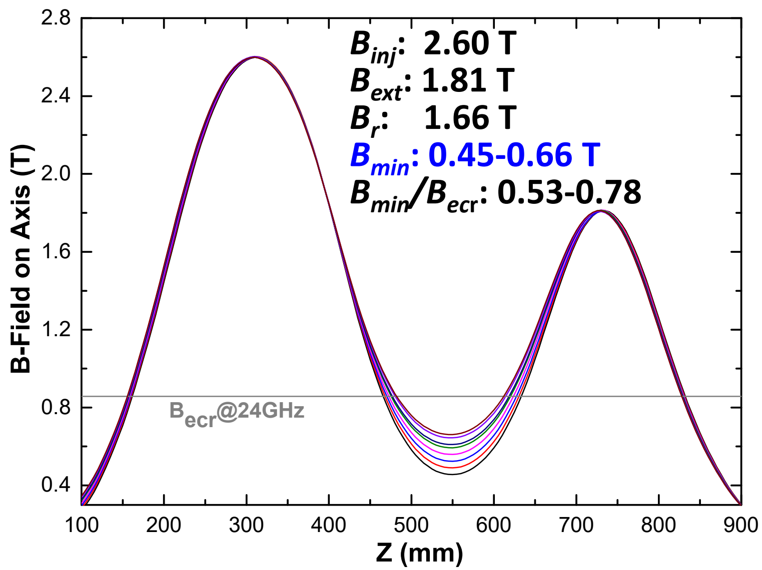

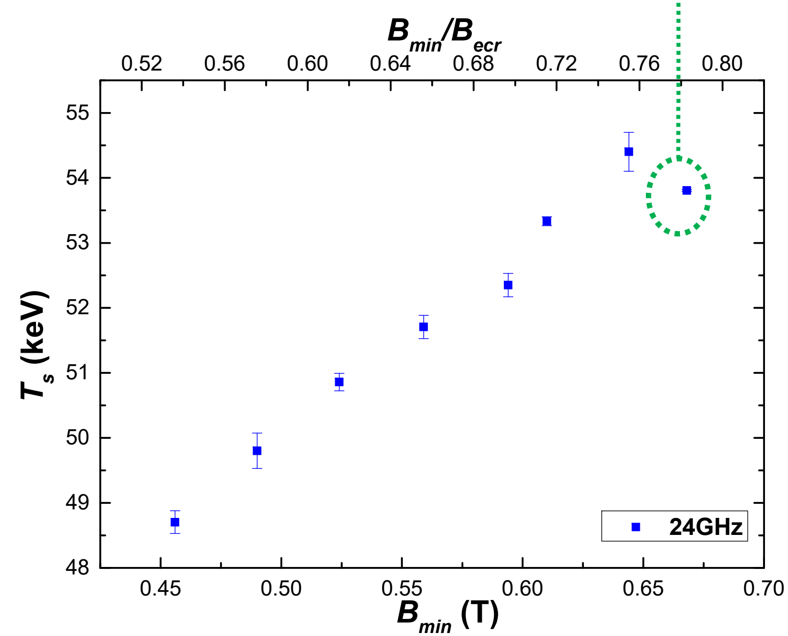

Experimental results- part 1
Constant B_{inj} , B_{ext} and B_r while varying B_{min}

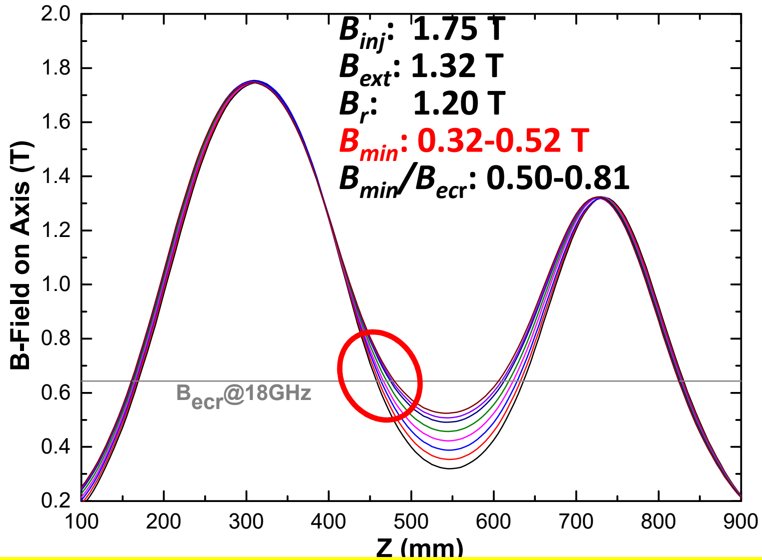

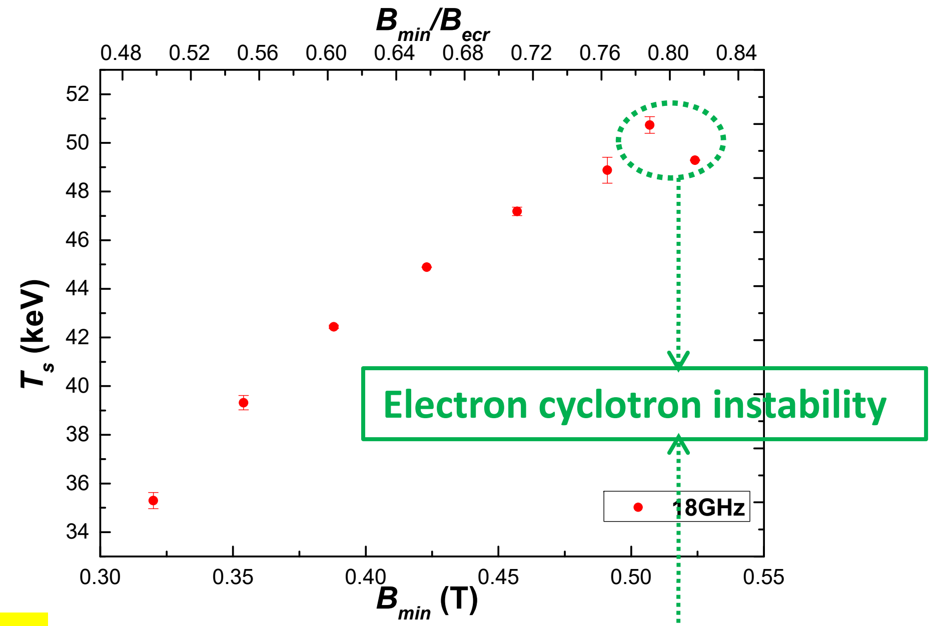

Note: on-axis ∇B_{ecr} is also changed when B_{min} is changed

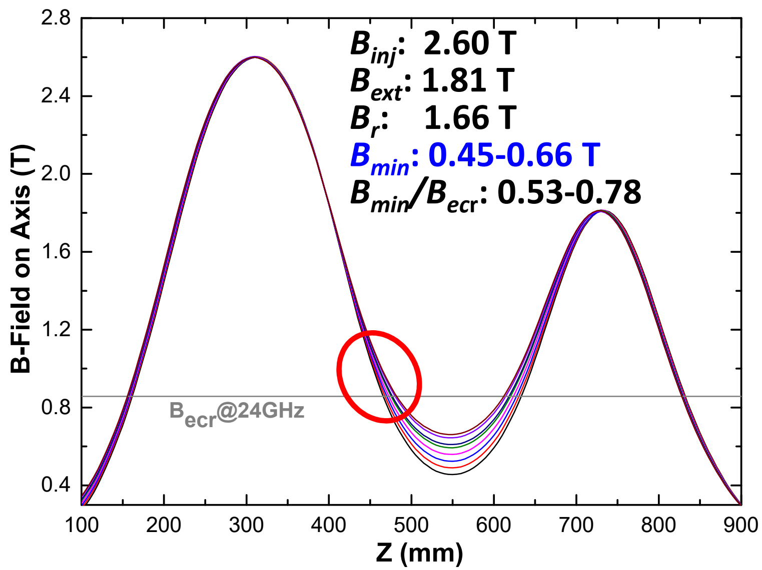

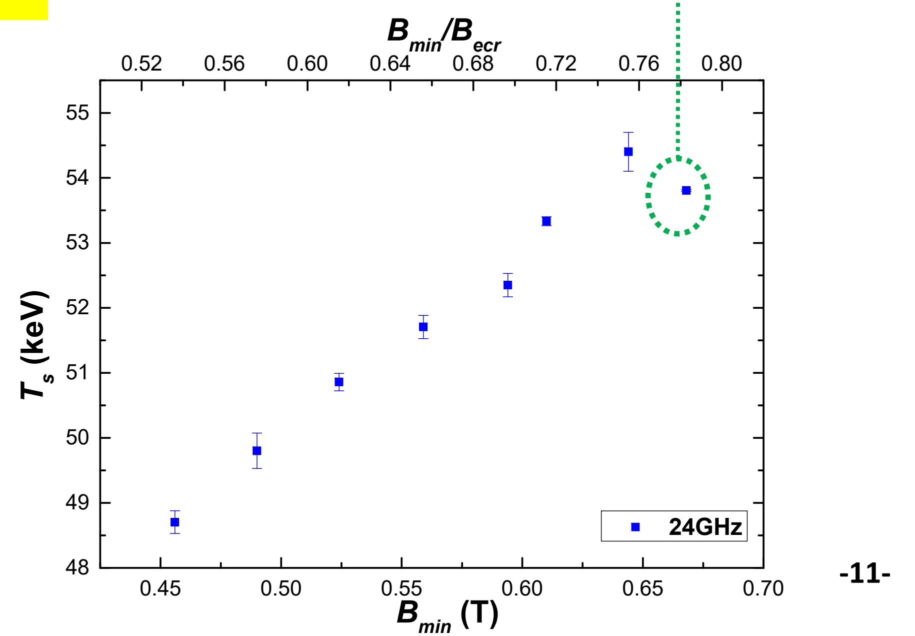

Experimental results- part 2

Constant on-axis ∇B_{ecr} and B_r while varying B_{min}

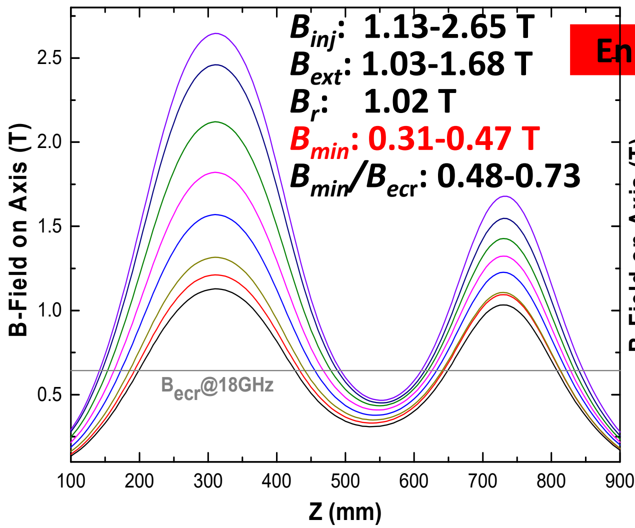

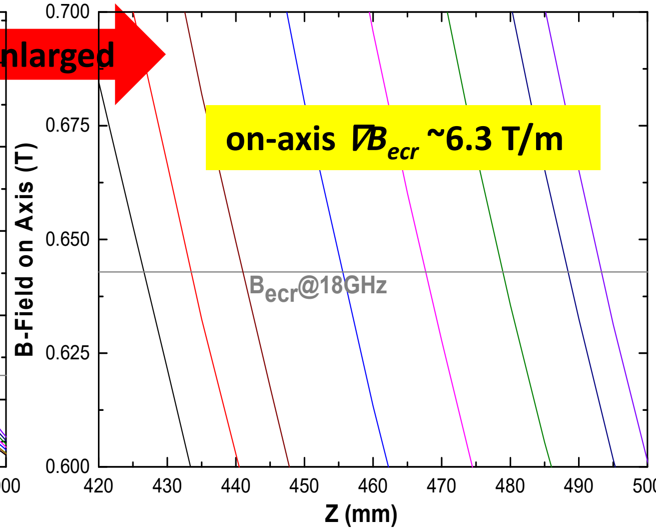

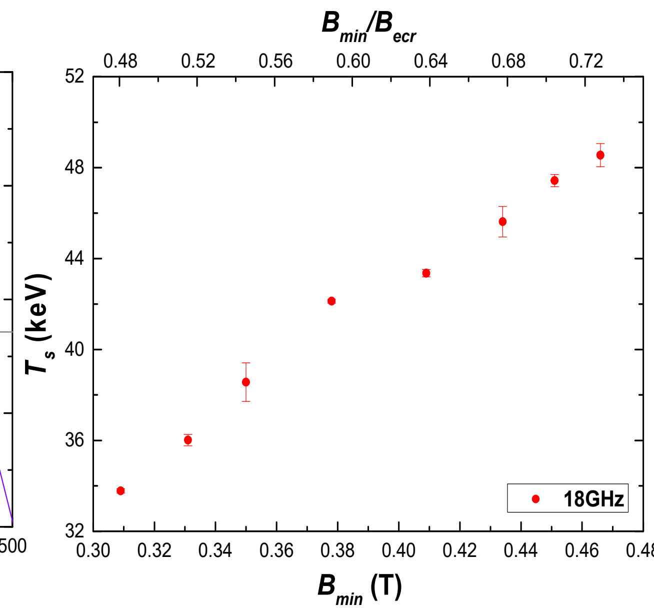

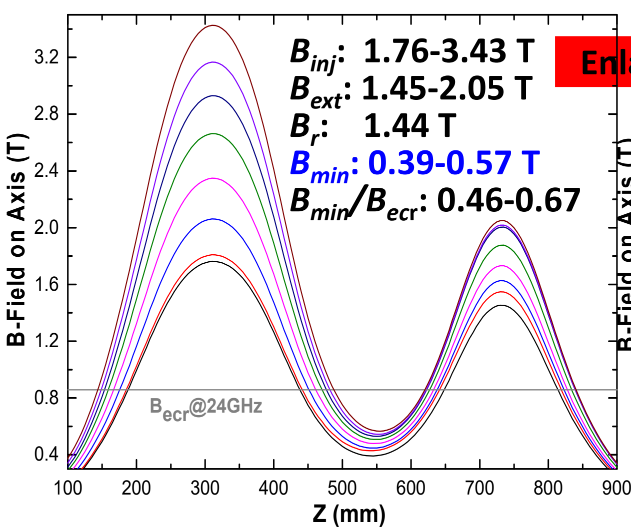

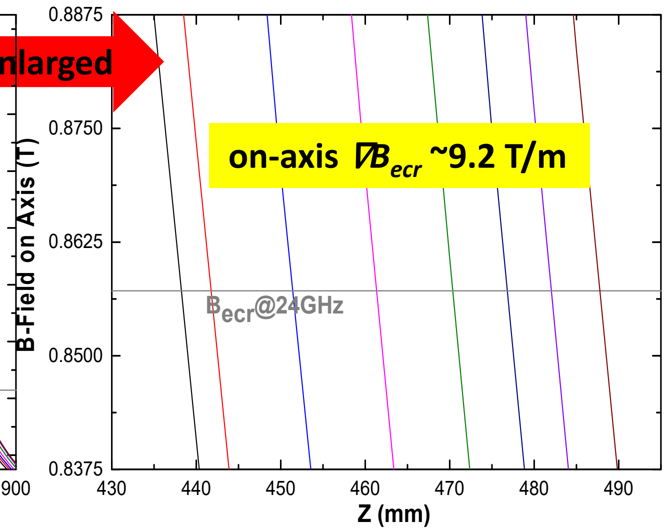

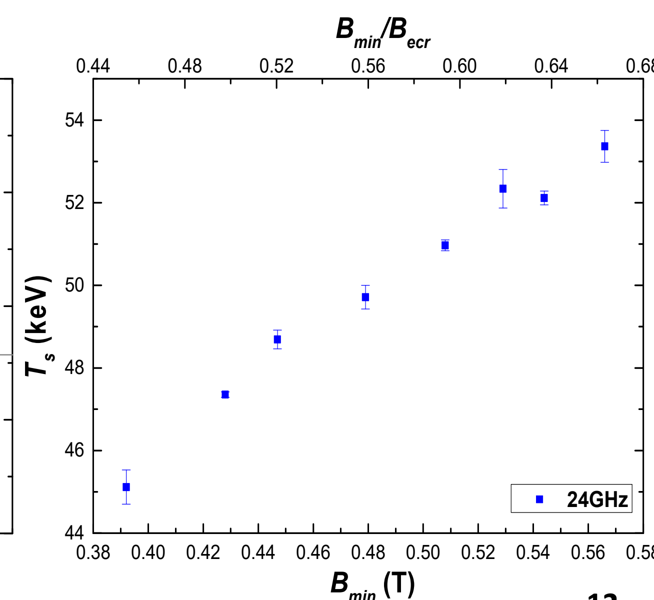

Experimental results- part 3

Constant B_{min} and B_r while varying on-axis ∇B_{ecr}

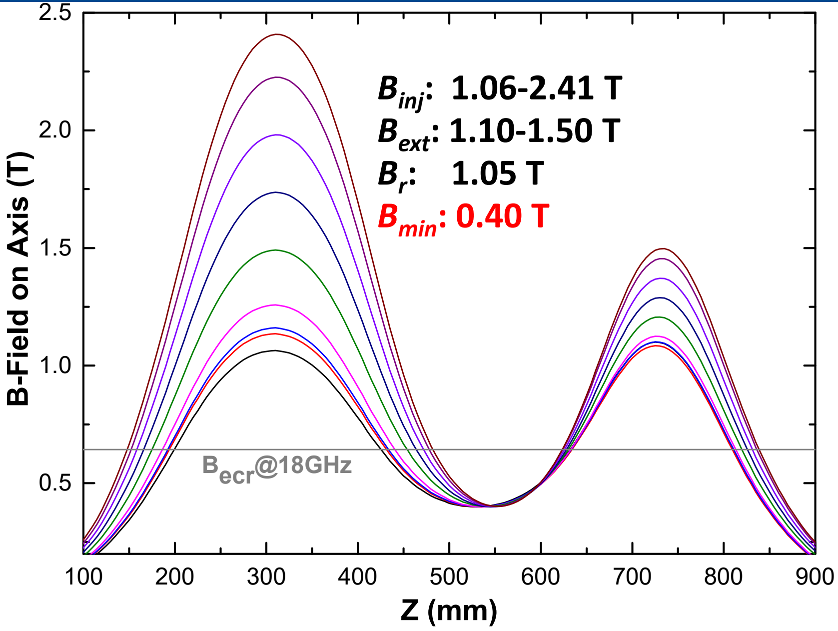

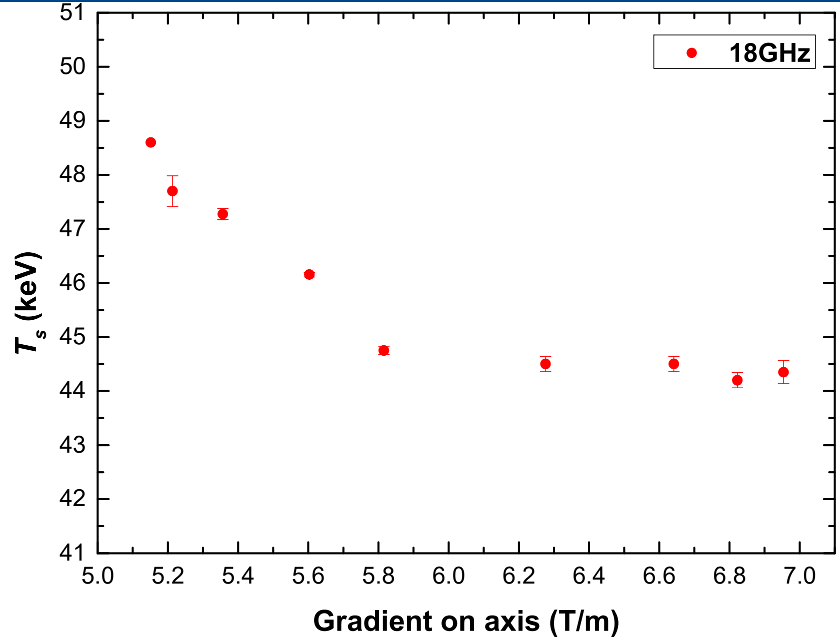

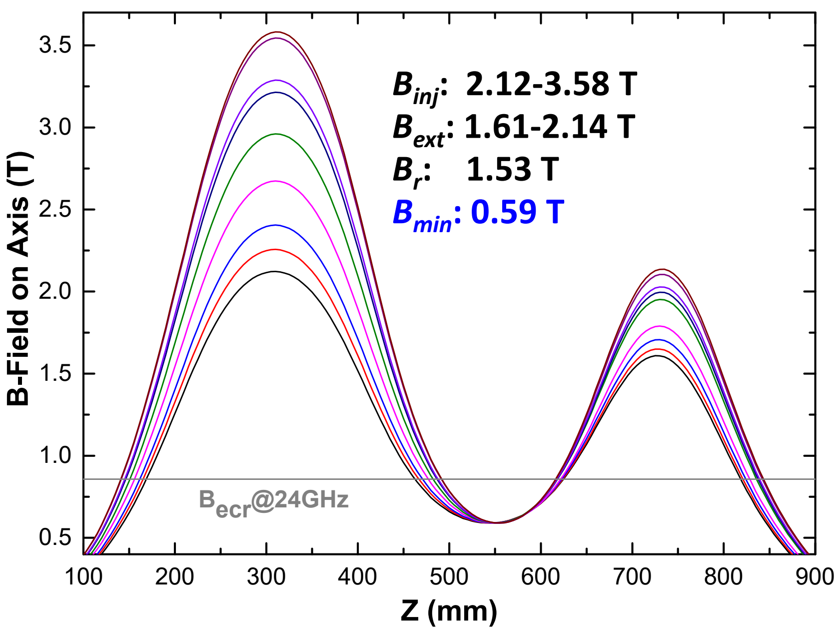

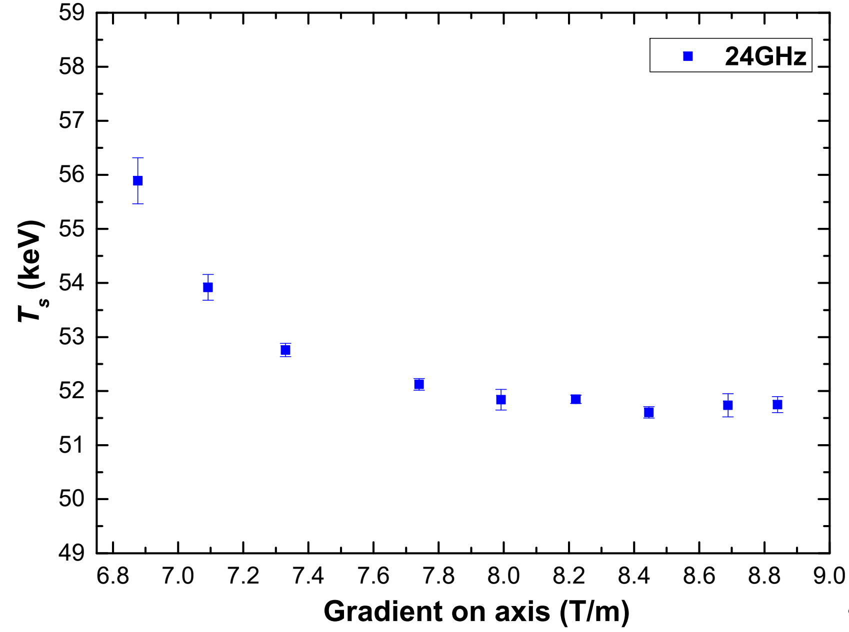

Experimental results- part 4
Constant B_{inj} , B_{ext} and B_{min} while varying B_r

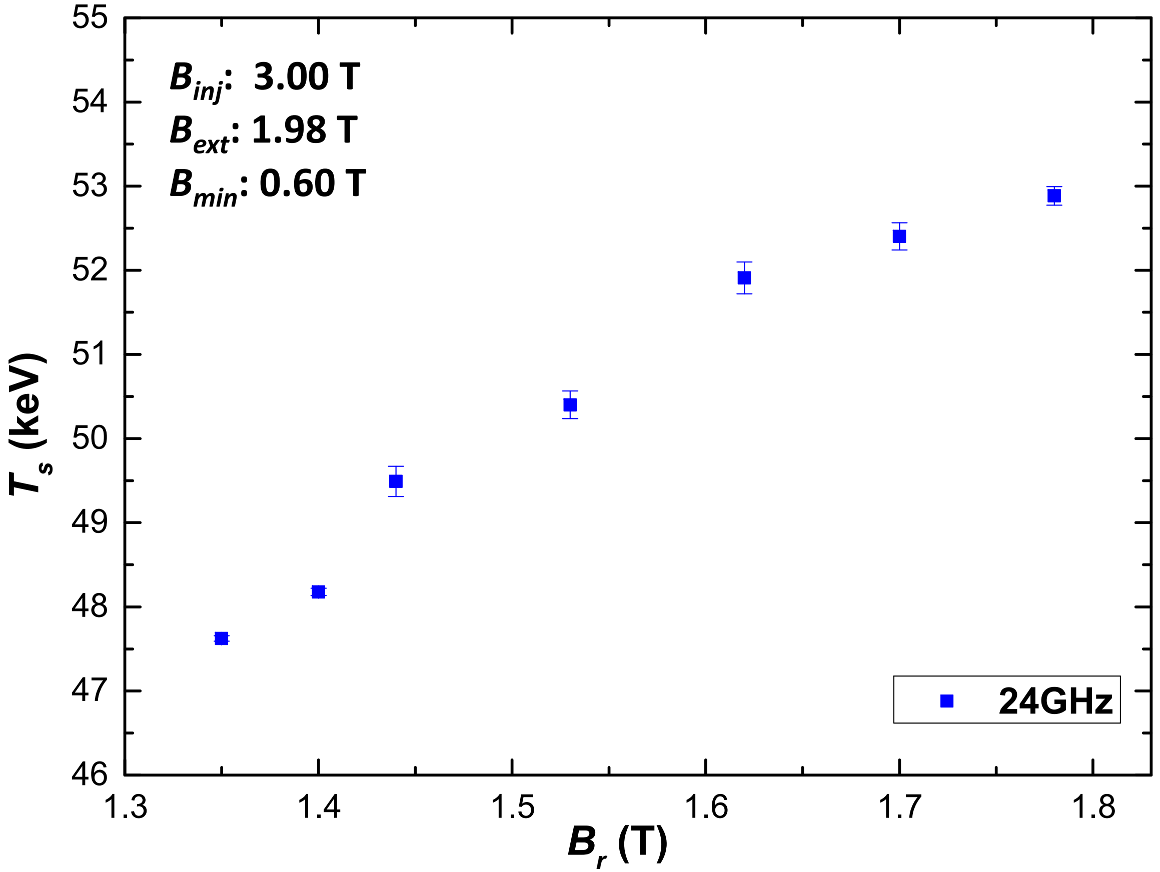

-Correlation between T_s and electron cyclotron instabilities

Summary of T_s versus B_{min}/B_{ecr}

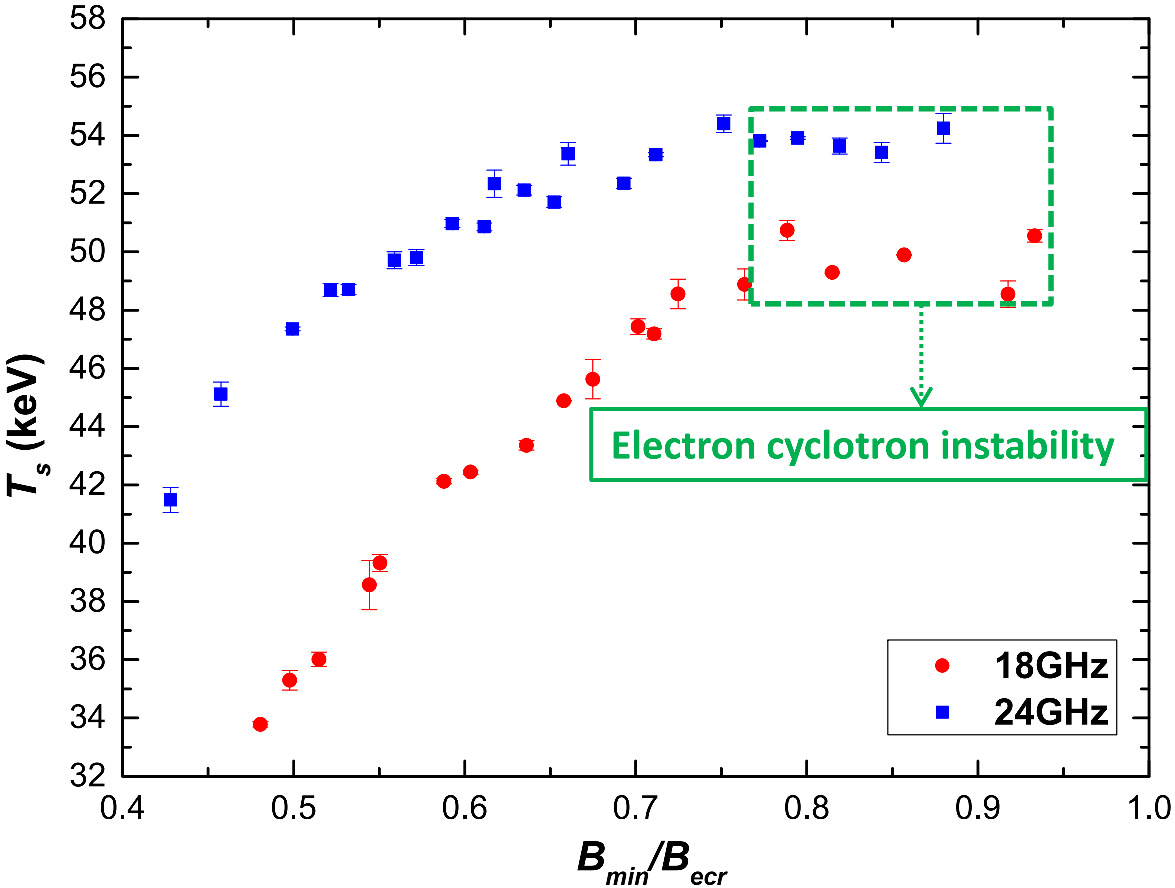

Discussion
-Correlation between T_s and electron cyclotron instabilities

Summary of T_s versus B_{min}/B_{ecr}

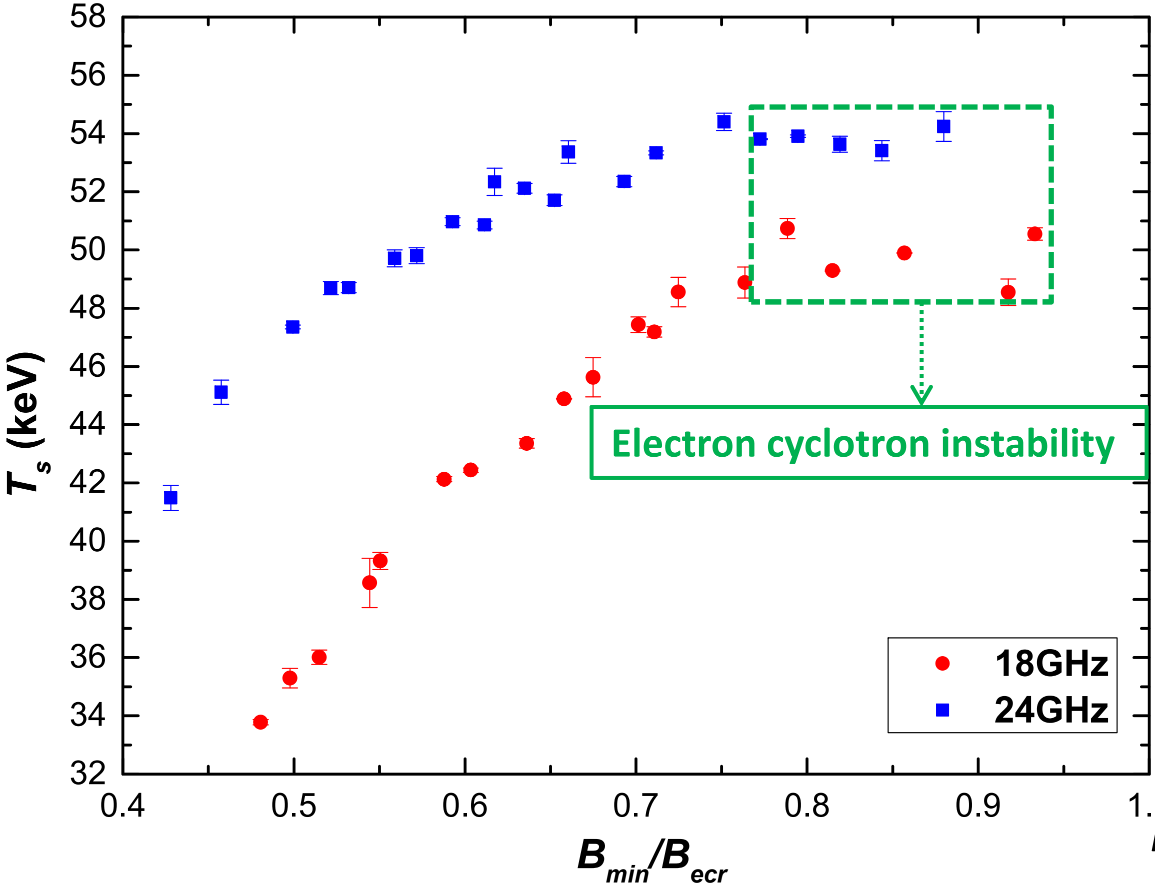

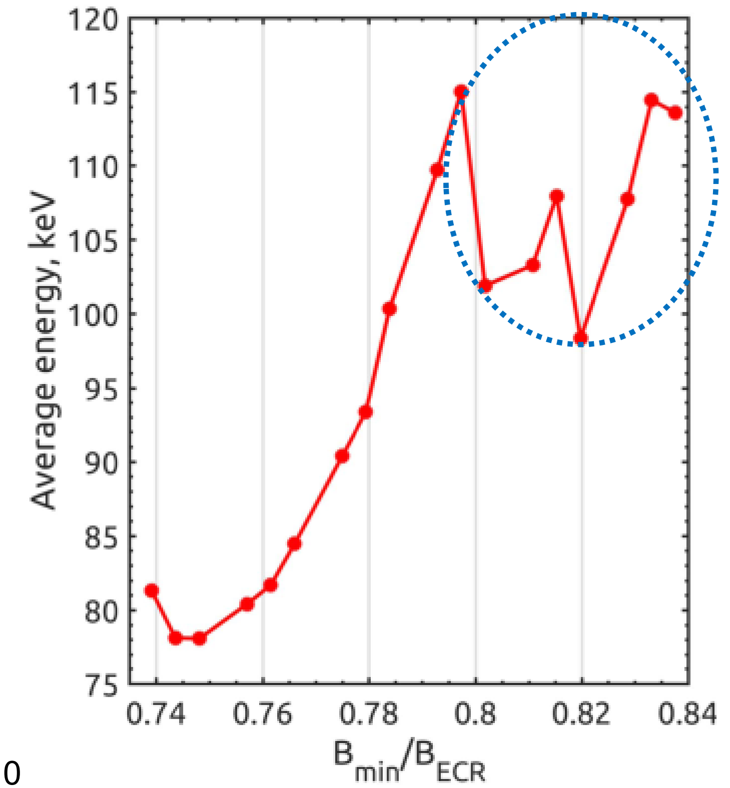

Izotov I et al 2018 Plasma Sources Sci. Technol. 27 025012

Discussion
-How to understand apparent linear B_{min} dependence on T_s

- ☐ Electron energy gain in single resonance crossing
- ☐ Effective resonance width

depend strongly on ∇B_{ecr} rather than B_{min}

Average gradient over ECR surface:

$$<\nabla B_{ecr}> = <\left(\vec{B}/\left|\vec{B}\right|\right)\cdot\nabla B>_{ecr,cold}$$

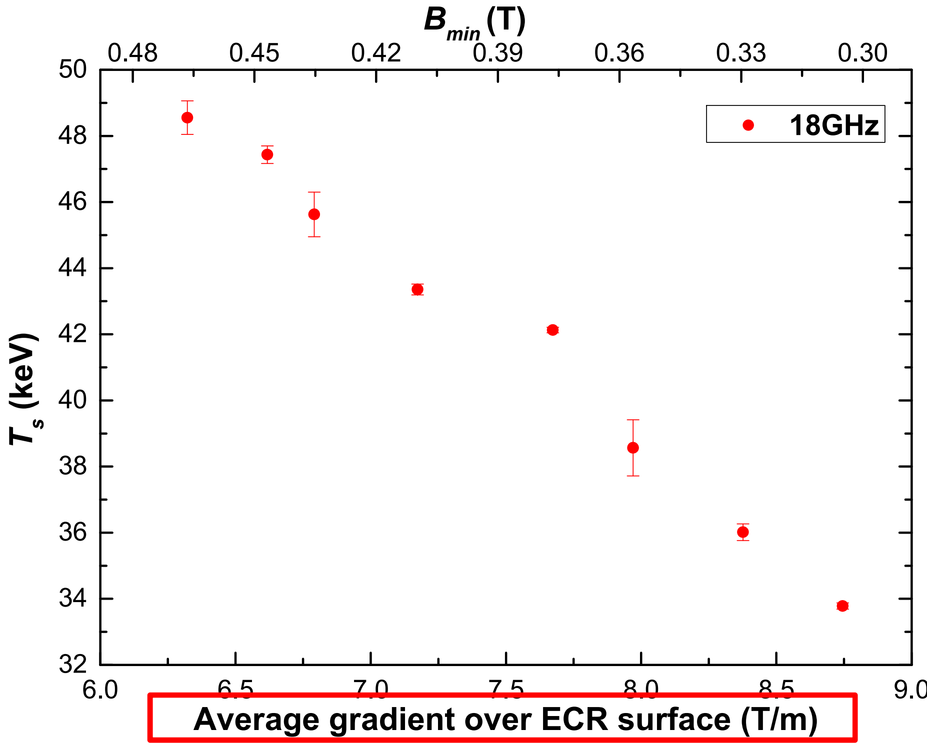

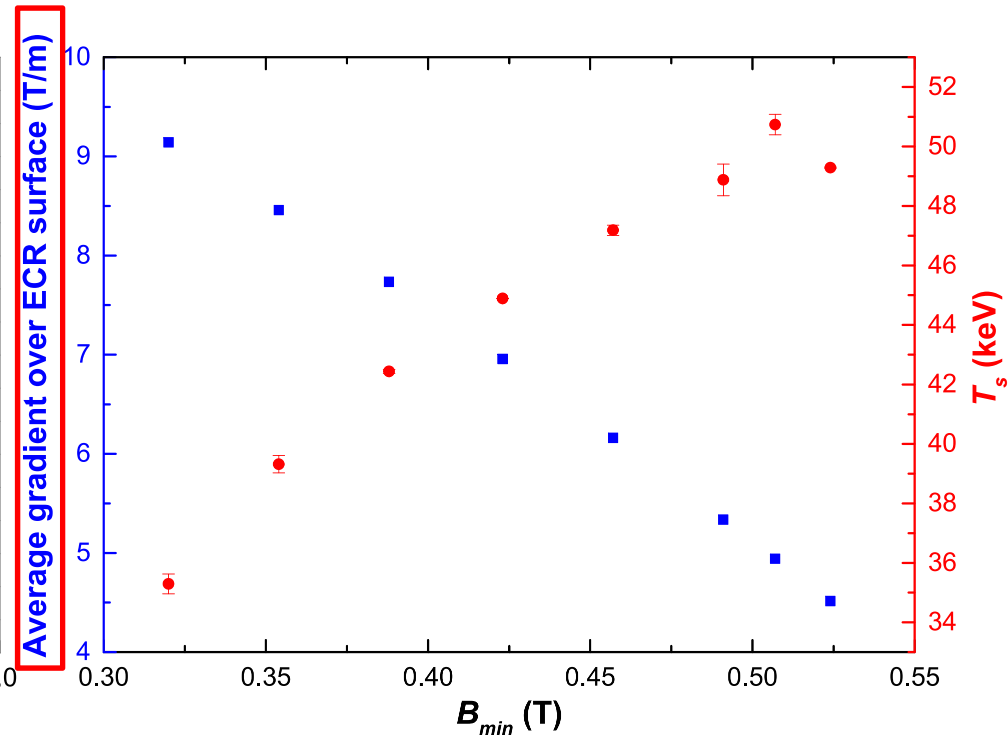

Constant on-axis ∇B_{ecr} and B_r while varying B_{min}

Constant B_{inj} , B_{ext} and B_r while varying B_{min}

Discussion
-Plasma confinement

Constant B_{min} and B_r while varying on-axis ∇B_{ecr}

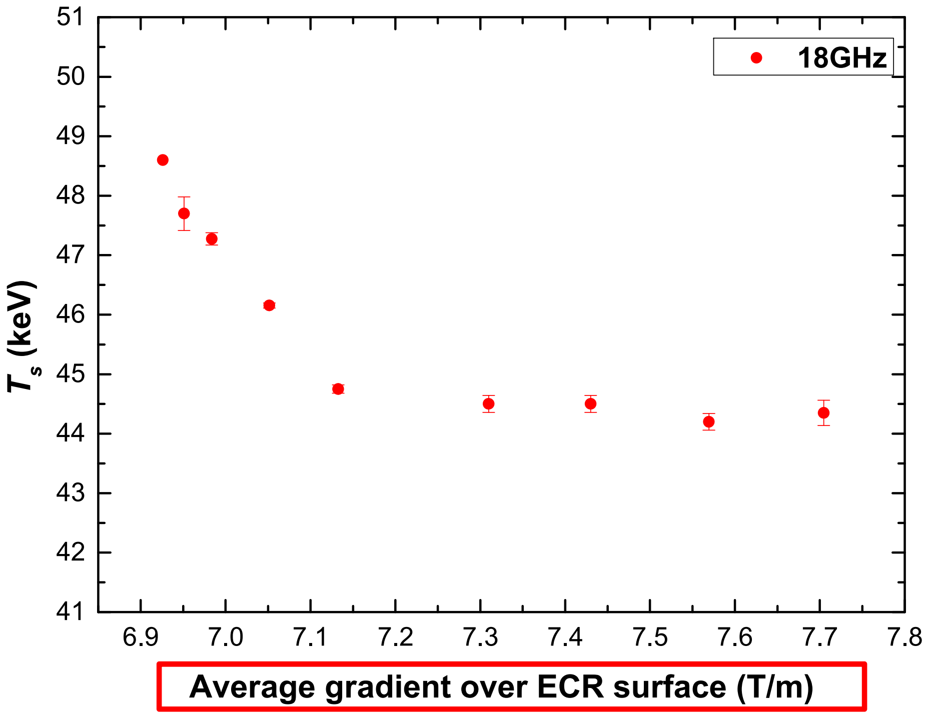

B_r (T)	B_{min} (T)	B_{inj} (T)	B_{ext} (T)	$< \nabla B_{ecr} >$ (T/m)
1.05	0.40	1.06	1.10	6.92
		1.14	1.11	6.95
		1.16	1.12	6.98
		1.26	1.13	7.05
		1.49	1.21	7.13
		1.74	1.29	7.31
		1.98	1.37	7.43
		2.23	1.45	7.57
		2.41	1.50	7.70

Mirror ratio (B_{max}/B_{min}): 2.65-6.03

Discussion
-Plasma confinement

Constant B_{inj} , B_{ext} and B_{min} while varying B_r

B_{last} defines overall magnetic confinement

f (GHz)	B_{inj} (T)	B_{min} (T)	B_{ext} (T)	B_r (T)	$< \nabla B_{ecr} >$ (T/m)	B_{last} (T)
24	3.00	0.60	1.98	1.35	9.09	1.05
				1.40	9.13	1.09
				1.44	9.18	1.13
				1.53	9.29	1.21
				1.62	9.39	1.29
				1.70	9.50	1.37
				1.78	9.61	1.45

Weak effect of $< \nabla B_{ecr} >$

Conclusion

I. **Bremsstrahlung spectral temperature T_s increases approximately linearly with the increase of B_{min}/B_{ecr} up to ~ 0.8 and then saturates with the appearance of electron cyclotron instabilities, which suggests that periodic bursts of energetic electrons escaping the magnetic confinement will limit the increase of the energy content carried by the hot electron population and eventually lead to a saturation of T_s;**

II. **Increasing B_{min} corresponds to decreasing $<\nabla B_{ecr}>$ although the on-axis ∇B_{ecr} remains constant, which shows the inherent link between B_{min} and $<\nabla B_{ecr}>$, and thus provides a viewpoint that is more coincident with theoretical studies to understand the apparent linear B_{min} dependence and the appearance of electron cyclotron instabilities;**

III. **T_s decreases with the increasing of gradient (on-axis ∇B_{ecr} and $<\nabla B_{ecr}>$) at relatively low mirror ratio and is insensitive to the gradient at high mirror ratio when B_{min} is constant, which indicates that T_s depends on not only electron heating, but also depends on electron confinement. This view is supported by the dependence of T_s on the radial confinement.**

Acknowledgement

- J. Benitez, LBNL
- D. Xie, LBNL

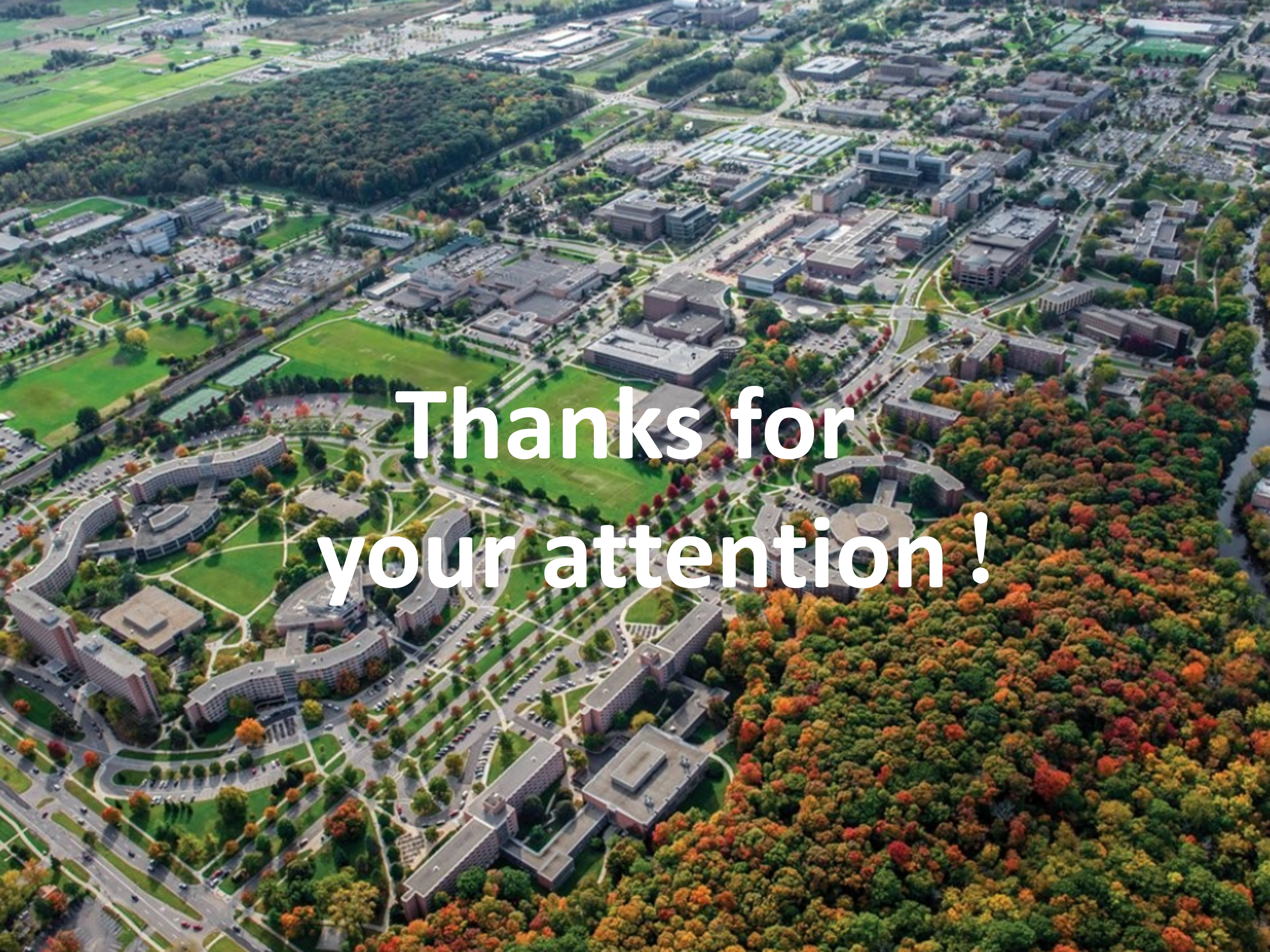
Thanks for
your attention !

Appendix

XR-100-CdTe Detector	
Detector type	Cadmium Telluride (CdTe) Diode
Detector areas	5 x 5 mm (25 mm^2)
Detector thickness	1 mm
Energy resolution @ 122 keV, ^{57}Co	<1.5 keV FWHM, typical
Detector window	Be: 4 mil thick (100 µm)
Energy range	10 – 300 keV
Detector efficiency	See below

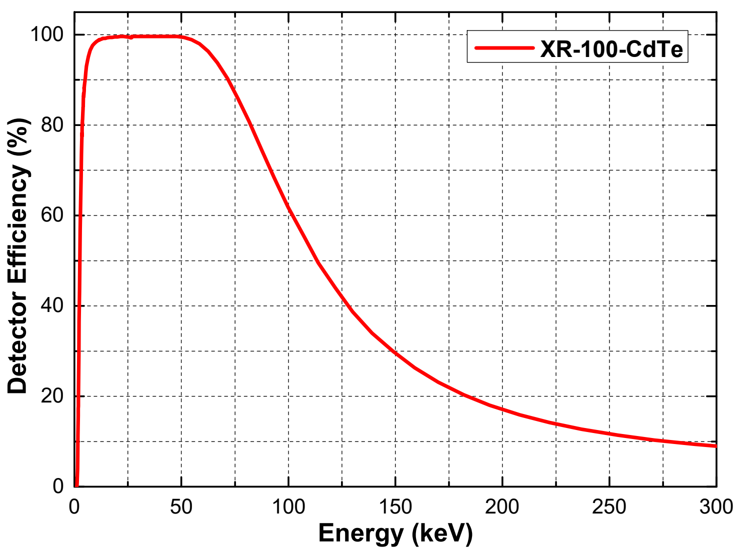

8473C Low-Barrier Schottky Diode Detector, 10 MHz to 26.5 GHz

Images

Sold By: Keysight - Usually arrives in 7 weeks
Authorized Sales Partners - Check availability

View Data Sheet

Visit Technical Support

Overview & Features | Options & Accessories | Document Library

Key Features & Specifications

Superior RF Performance

- Frequency response: ±0.3 dB to 12.4 GHz, ±0.6 dB to 20 GHz, ±1.5 dB from a -3.3 dB linear slope starting at 20 GHz to 26.5 GHz
- Maximum SWR: 1.2 to 4 GHz, 1.5 to 18 GHz, 2.2 to 26.5 GHz
- Low-level sensitivity: > 0.5 mV/uW to 18 GHz, > 0.18 mV/uW to 26.5 GHz
- Maximum operating input power: 200 mW
- Typical short-term maximum input power (< 1 minute): 1 W
- Noise: < 50 uV
- Output polarity: negative
- Input connector: 3.5 mm male

Description

The Keysight 8473C Low-Barrier Schottky Diode (LBSD) detector has been widely used for many years in a variety of applications including leveling and power sensing . It offers good performance and ruggedness. Matched pairs (Option 001) offer very good detector tracking.

Appendix

Efficiency of Collimating System

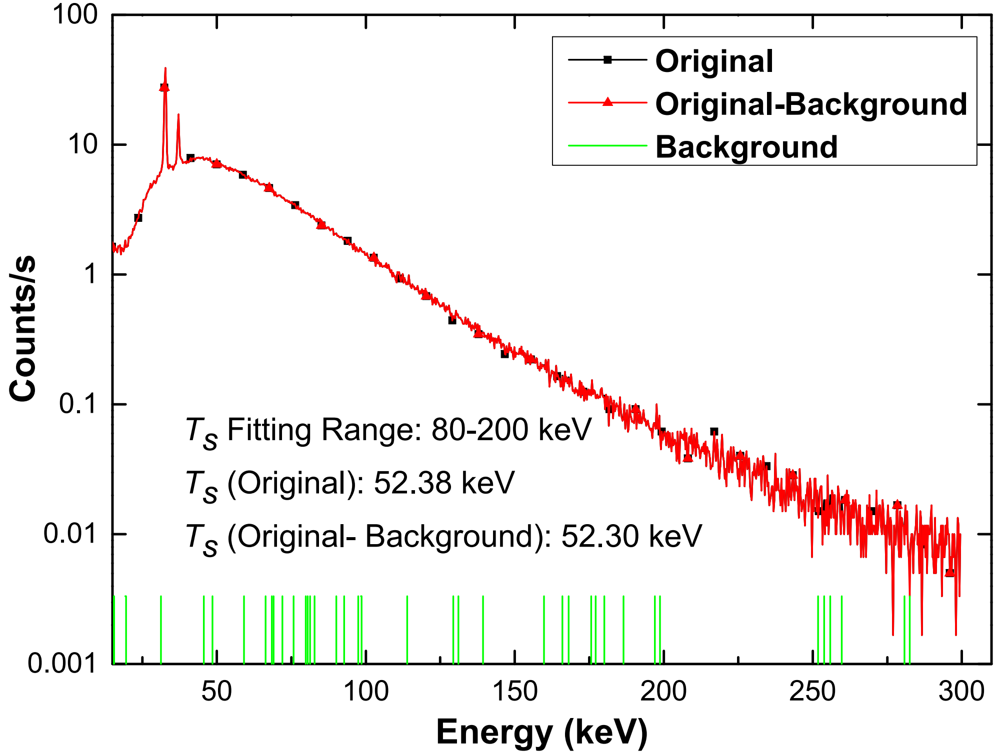

- Difference (with or without background subtraction) of T_S is less than 0.16%
- All data presented in this talk are spectra without background subtraction

Appendix

The solenoid field model is constructed by fitting a sixth order polynomial Bz(z) to on axis magnetic field

The off-axis solenoid field is evaluated with a standard expansion

$$\begin{aligned} B_z(r,z) &= A_0 + A_1 z + A_2\left(z^2 - \frac{r^2}{2}\right) + A_3\left(z^3 - \frac{3r^2 z}{2}\right) \\ &+ A_4\left(z^4 - 3r^2 z^2 + \frac{3r^4}{8}\right) + A_5\left(z^5 - 5r^2 z^3 + \frac{15r^4 z}{8}\right) \\ &+ A_6\left(z^6 - \frac{15r^2 z^4}{2} + \frac{45r^4 z^2}{8} - \frac{5r^6}{16}\right), \qquad \text{(A1)} \end{aligned}$$

$$\begin{aligned} B_r(r,z) &= -A_1\frac{r}{2} - A_2 r z - A_3\left(\frac{3rz^2}{2} - \frac{3r^3}{8}\right) \\ &- A_4\left(2rz^3 - \frac{3r^3 z}{2}\right) - A_5\left(\frac{5rz^4}{2} - \frac{15r^3 z^2}{4} + \frac{5r^5}{16}\right) \\ &- A_6\left(3rz^5 - \frac{15r^3 z^3}{2} + \frac{15r^5 z}{8}\right), \qquad \text{(A2)} \end{aligned}$$

The sextupole field model is constructed by fitting a linear combination of cylindrical multipoles

$$B_r(r,\theta) = \sum_i J_i \left(\frac{r}{r_{\mathrm{ref}}}\right)^{i-1} \cos(i\theta), \qquad \text{(A3)}$$

$$B_\theta(r,\theta) = \sum_i -J_i \left(\frac{r}{r_{\mathrm{ref}}}\right)^{i-1} \sin(i\theta), \qquad \text{(A4)}$$